

**PROJECT #2015-012**

DATE: July 7-9, 2015

## **Two-Layer In-Situ Performance Comparison of TX130s and BX1200 Geogrid Stabilized Aggregate Layer over Soft Subgrade: Boone Test Bed, Boone, IA USA**

By

David J. White, Ph.D., P.E.

*Ingios Geotechnics, Inc.*



Prepared for Tensar International Corporation, Alpharetta, GA

---

## Executive Summary

At the request of Tensar Corporation, Ingios Geotechnics, Inc. conducted automated plate load tests (APLTs) on a test pad constructed in Boone, Iowa, with two different geogrid products (TX130s and BX1200). The test sections were about 12 ft long by 60 ft wide and consisted of 6 in. of crushed limestone base (classified as GP-GM; A-1-a) over relatively uniform and soft natural subgrade material (classified as CL) with California bearing ratio (CBR) of 0.7 to 2.3, with geogrids placed at the base/subgrade interface. Tests were also conducted on a reference control test section with no geogrid.

Cyclic APLTs were conducted in seven loading sequences, with 100 cycles in each loading sequence. Cyclic stresses varied from 3 psi to 100 psi. Tests were conducted at one test location in each section using a 12 inch diameter plate, including a sensor kit to measure ground deflections at selected radial distances from the plate center. The cyclic test results were used to determine composite, stabilized base, and subgrade layer resilient modulus ( $M_r$ ) values, and assess permanent and resilient deformation characteristics. Dynamic cone penetration tests (unconfined surface) were performed at each cyclic APLT test location to determine penetration resistance and CBR profiles up to a depth of about 2.5 ft below surface. Sand cone tests were conducted at the surface at each APLT test location to determine dry unit weight and moisture content of the base layer material. Photographs documented the surface conditions and the base/subgrade layer interface after cyclic loading.

Laboratory tests were conducted on the aggregate base and subgrade material to determine soil index properties and laboratory  $M_r$  properties.  $M_r$  test results obtained from laboratory were compared with the field test results.

The control sections showed the highest permanent deformation ( $\delta_p$ ) with 1.1 to 1.5 in. at the end of 700 cycles. The TX130s section showed the lowest  $\delta_p$  ( $< 0.5$  in.) while the BX1200 section showed  $\delta_p = 0.75$  in., at the end of 700 cycles.

The TX130s section showed higher TBR values (4.1 to 5.4) than the BX1200 section (1.6 to 1.9) at  $\sigma_{\text{cyclic}} \geq 37$  psi. The TBR values determined from APLT testing in the TX130s section are comparable to the TBR values measured from the 2012 truck trafficking testing. The TBR values from APLT testing in the BX1200 section, however, were lower than measured from the truck trafficking testing.

In the Control 2 section,  $\delta p$  at 2r and 3r resulted in vertical heaving. Results from the remaining sections showed that there was little  $\delta p$  outside the perimeter of the loading plate. This is indicative of soft subgrade conditions where the plate deformations are governed significantly by permanent deformations in the subgrade layer.

The permanent deformation basin values analyzed in terms of relative movements indicated that both TX130s and BX1200 geogrid sections were in near-linear elastic/compression mode while the control sections were in plastic deformation/heave mode. The Control 2 section produced the most heave in the deflection basin region and the TX130s produced the most compression in the deflection basin region. This observation provides new understanding of the geogrid-subgrade-subbase interaction.

The composite  $M_r$  and  $M_{r(\text{sg})}$  and  $M_{r(\text{Base})}$  values calculated from layered analysis, all decreased with increased cyclic stresses. This behavior was observed in laboratory  $M_r$  testing on the subgrade material. The opposite was observed for the aggregate laboratory resilient modulus test. The composite  $M_r$  values at  $\sigma_{\text{cyclic}} = 98$  psi ranged between 6.1 ksi and 8.7 ksi in all sections. The composite  $M_r$  values were similar to the  $M_{r(\text{sg})}$  values in all sections, especially at  $\sigma_{\text{cyclic}} > 30$  psi, which suggests that the composite behavior is dominated by the subgrade layer stiffness.

Additional testing is recommended for a moderate subgrade stiffness (CBR 3-7).

**DISCLAIMER:**

Ingios Geotechnics, Inc. and its Affiliates disclaim any and all responsibility and liability for the use of any such data, information and/or the analysis presented in this report. Although Ingios Geotechnics, Inc. takes all possible care to ensure the correctness of published information, no warranty can be accepted regarding the correctness, accuracy, uptodateness, reliability and completeness of the content of this information.

Ingios Geotechnics, Inc. expressly reserves the right to change, to delete or temporarily not to publish the contents wholly or partly at any time and without giving notice. Liability claims against Ingios Geotechnics, Inc. because of tangible or intangible damage arising from accessing, using or not using the published information, through misuse of the contents or as a result of technical breakdowns are excluded.

# Contents

<b>Executive Summary .....</b>	<b>ii</b>
<b>1 Introduction .....</b>	<b>1</b>
1.1 Background.....	1
1.2 Objective.....	2
1.3 Scope.....	2
<b>2 Test Methods .....</b>	<b>3</b>
2.1 Automated Plate Load Test (APLT).....	3
2.1.1 Composite Resilient Modulus.....	5
2.1.2 Layered Analysis .....	6
2.1.3 Permanent Deformation Monitoring.....	9
2.2 Dynamic Cone Penetration (DCP) Testing.....	10
2.3 In Situ Moisture and Density Testing.....	10
2.4 Laboratory Testing.....	11
2.4.1 Soil Index Properties .....	11
2.4.2 Resilient Modulus .....	12
<b>3 Experimental Study.....</b>	<b>14</b>
3.1 Field Experimental Study .....	14
3.2 Project Details.....	15
3.2.1 Test Section Construction and 2012 Testing.....	15
3.2.2 2015 Testing.....	16
3.3 Material Properties and Laboratory Test Results .....	17
<b>4 Results.....</b>	<b>22</b>
4.1 Dynamic Cone Penetration (DCP) Test Results.....	22
4.2 Comparison of APLT Permanent Deformation Basins and Power Models.....	23
4.3 In-Situ Resilient Modulus .....	27
<b>5 Conclusions and Recommendations.....</b>	<b>31</b>
<b>References.....</b>	<b>33</b>

## Figures

Figure 1. APLT test system.....	4
Figure 2. Example output from APLT test system.....	4
Figure 3. APLT test setup with deformation measurements obtained at 2 <i>r</i> , 3 <i>r</i> , and 4 <i>r</i> from the plate center axis.....	7
Figure 4. Illustration of Odemark’s MET concept. ....	8
Figure 5. Picture of an excavated hole ready for sand cone testing. ....	11
Figure 6. Pictures of geogrids used in this study during construction of test sections in 2012: (a) BX1200 and (b) TX130s (field of view for each image about 4 inches). ....	15
Figure 7. Vibratory compaction of aggregate base layer prior to APLT for uniform and level testing surface .....	16
Figure 8. Aggregate base layer surface at the time of testing .....	17
Figure 9. APLT setup showing 12 in. diameter plate and the 2 <i>r</i> , 3 <i>r</i> , and 4 <i>r</i> deflection basis measurement rings.....	17
Figure 10. Grain-size analysis and classification of the crushed limestone aggregate base material.....	18
Figure 11. (top) Full gradation sample and (bottom) gravel retained on No. 4 sieve after washing and oven-drying for the crushed aggregate base material .....	19
Figure 12. Grain-size analysis and classification of the subgrade material directly beneath the aggregate base .....	20
Figure 13. Results of laboratory $M_r$ testing on subgrade sample and prediction equations based using $k-\sigma_d$ and $k_1-k_3$ constitutive models.....	21
Figure 14. Results of laboratory $M_r$ testing on aggregate base and prediction equations based using $k-\theta$ and $k_1-k_3$ constitutive models.....	21
Figure 15. DCP profiles for all test locations.....	22
Figure 16. Permanent deformation at 1 <i>r</i> versus load cycle number at all test points.....	24
Figure 17. Permanent deformation at 2 <i>r</i> versus load cycle number at all test points.....	24
Figure 18. Permanent deformation at 3 <i>r</i> versus load cycle number at all test points.....	25
Figure 19. Permanent deformation at 4 <i>r</i> versus load cycle number at all test points.....	25
Figure 20. Permanent deformation basins at all test points at the end of each load sequence.....	26
Figure 21. Ratio of vertical permanent deformation with distance from plate edge showing near-linear elastic compression and plastic deformation modes at end of 500 cycle test sequence. ....	26
Figure 22. Resilient deformation basins at all test points at the end of each load sequence.....	28

Figure 23. Summary of aggregate layer thicknesses and in-situ measurement values.....30

---

## Tables

Table 1. Summary of plate tests and configurations. ....	14
Table 2. Summary of geogrid mechanical properties. ....	14
Table 3. Summary of TBR in the geogrid stabilized sections from 2012 trafficking tests. ....	16
Table 4. Summary of permanent deformation prediction parameters. ....	27
Table 5. Comparison of test results for in-situ $M_r$ and permanent deformation testing. ....	29

---

# 1 Introduction

## 1.1 Background

The static plate load test (AASHTO T222) has been widely used in different geotechnical engineering fields and particularly in the characterization of foundation layer properties for rigid pavements. The strain or deformation modulus ( $E_v$ ) is commonly used in pavement design in Europe, while the resilient modulus is used in the U.S. The strain modulus,  $E_{V2}$  is calculated from the second loading cycle using the Boussinesq solution and secant method (DIN 18134, 2001). In contrast, resilient modulus ( $M_r$ ) is determined using *resilient* deflection of materials after many stress cycles. Resilient modulus can be obtained from the laboratory triaxial test (e.g., per AASHTO T307, 2000 or NCHRP, 2004). However, due to the complexity of the laboratory triaxial test and often non-representative boundary conditions, the resilient modulus of pavement foundation materials is often obtained from empirical correlations between resilient modulus and other properties such as soil classification, California Bearing Ratio (CBR) or Hveem R-value.

In-situ resilient modulus is also predicted from non-destructive surrogate tests including the falling weight deflectometer (FWD) or light weight deflectometer (LWD). In practice, elastic moduli values calculated from these test devices based on *elastic* deformations are often confused with resilient modulus values which is based on *resilient* (i.e., recoverable) deformations.

One of the major limitations of these non-destructive surrogate tests is the lack of a conditioning stage prior to testing. During pavement construction, pavement foundation materials are subject to relatively high loads from construction traffic and compaction equipment. In response to these loads, aggregate particles rearrange themselves resulting in higher density and stiffness. For mechanically stabilized layers, this results in greater interlock and aggregate confinement. For this reason, it is important to apply conditioning load cycles prior to testing to determine in-situ resilient modulus. Once surface paving is complete, the pavement foundation below is confined by the overlying pavement layers. The response of a pavement foundation to subsequent repeated traffic loading is both nonlinear and stress-dependent and therefore the effect of confinement is an important

condition to consider in a field based resilient modulus test. In response to this need, the Automated Plate Load Test (APLT) system was designed to directly measure the influence of load cycles and confining pressure on in-situ resilient modulus and permanent deformation of the pavement foundation.

## 1.2 Objective

The objective of this study was to conduct cyclic APLTs to determine in-situ  $M_r$  and deformation characteristics and compare field performance of TX130s and BX1200 geogrid stabilized aggregate base over soft subgrade test sections. The geogrid test sections were constructed in 2012, along with a reference control test section with no geogrid.

## 1.3 Scope

Cyclic APLTs were conducted with cyclic stresses ranging between 3 psi and 100 psi in seven loading sequences, with 100 cycles in each loading sequence. Tests were conducted at one test location in each section using a 12 inch diameter plate, including a sensor kit to measure ground deflections at selected radial distances from the plate center. The cyclic test results were used to determine composite, stabilized base, and subgrade layer  $M_r$  values, and assess permanent and resilient deformation characteristics.

Dynamic cone penetration tests (unconfined surface) were performed at each cyclic APLT test location to determine penetration resistance and California bearing ratio (CBR) of profiles up to a depth of about 2.5 ft below surface. Sand cone tests were conducted at the surface at each APLT test location to determine dry unit weight and moisture content of the base layer material. Photographs documented the surface conditions and the base/subgrade layer interface after cyclic loading.

Laboratory tests were conducted on the aggregate base and subgrade material to determine soil index properties and laboratory  $M_r$  properties.  $M_r$  test results obtained from laboratory were compared with the field test results.

Results from this field study were evaluated with truck trafficking results obtained in 2012 shortly after the test sections were constructed.

---

## 2 Test Methods

### 2.1 Automated Plate Load Test (APLT)

For rapid field assessment of critical performance parameters, Automated Plate Load Test (APLT) equipment was developed by Dr. David J. White (U.S. and International Patents Pending). The APLT equipment was specifically developed to perform rapid field testing of pavement foundations, embankments, stabilized materials. The APLT equipment is capable of measuring the following:

- Modulus of subgrade reaction
- Confining stress dependent resilient modulus
- Strain modulus
- Permanent deformation
- Bearing capacity
- Undisturbed tube sampling and extrusion
- Shear wave velocity/modulus
- Cone penetration testing
- Borehole shear testing
- Rapid in-situ permeability

Figure 1 shows the plate load test equipment mounted on a trailer unit and Figure 2 is an example of the data out-put including the stress cycles, cyclic and permanent deformation, stress-displacement relationship, number of load cycles, and in-situ resilient modulus. The APLT unit is automated using electric-hydraulic control systems.



Figure 1. APLT test system.

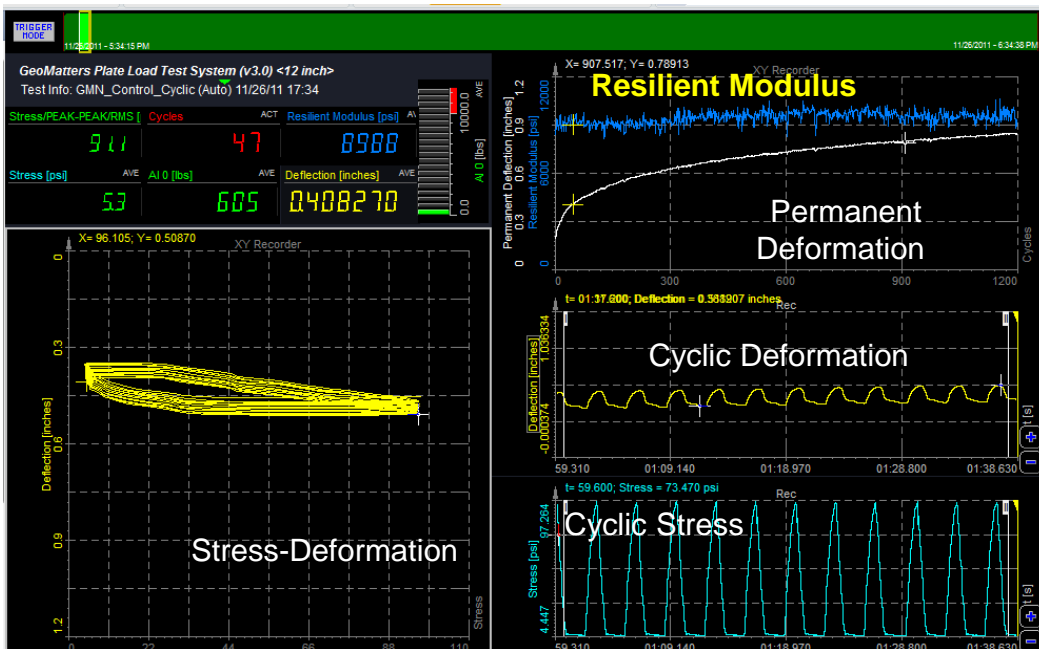


Figure 2. Example output from APLT test system.

### 2.1.1.1 Composite Resilient Modulus

The in-situ composite  $M_r$  was calculated as the ratio of the cyclic stress divided by the resilient deflection (during unloading) using the Boussinesq's half-space equation:

$$M_r = \frac{(1-\nu^2) \cdot \Delta\sigma_p \cdot r}{\delta_r} \times f \quad (1)$$

where,

$M_r$  is in-situ composite resilient modulus (uncorrected),

$\delta_r$  is the resilient deflection of plate during the unloading portion of the cycle (determined as the average of three measurements along the plate edge, i.e., at a radial distance  $r' = r$ ),

$\nu$  is the Poisson ratio (assumed as 0.40),

$\Delta\sigma_p$  is the cyclic stress,

$r$  is the radius of the plate,

$f$  is the shape factor selected as 8/3 for rigid plate on granular material.

In reality, Poisson's ratio will vary between test sections due to the aggregate stabilization mechanism(s) and loading conditions. Several papers in the literature demonstrate that this value can vary from 0.1 to 1+ due to the stress level and volume change characteristics (e.g., Brown et al. 1975, LeKarp et al. 2000).

Corrections to the measured in-situ composite  $M_r$  can be made as shown in Eq. (2) for plate bending ( $F_{Bending}$ ), plate size ( $F_{PlateSize}$ ), and the effect of future saturation ( $F_{Saturation}$ ) in the subgrade:

$$M'_r = \frac{(1-\nu^2) \cdot \Delta\sigma_p \cdot r}{\delta_r} \times f \times F_{Bending} \times F_{PlateSize} \times F_{Saturation} \quad (2)$$

In this report, no corrections were made for plate bending (i.e.,  $F_{Bending}$  is assumed as 1). The 12 inch diameter plate was 1 in. thick with a 6 in. diameter plate that is 1 in. thick and a carriage plate. Further, no corrections were applied for future saturation conditions (i.e.,  $F_{Saturation}$  is 1).

Plate size corrections are often considered in field evaluations as the influence depths change with different plate sizes (typically assumed as twice the plate diameter). There is also a scale effect that is a function of the plate circumference to plate area ratio.

According to ASTM D1195-93 (2004) and AASHTO T221-90 (2012) for repetitive static plate load tests of soil and flexible pavement components:

*“...For evaluation purposes alone, a single plate may be used, provided that its area is equal to the tire-contact area corresponding to what may be considered as the most critical combination of conditions of wheel load and tire pressure. For the purpose of providing data indicative of bearing index (for example, the determination of relative subgrade support throughout a period of a year), a single plate of any selected size may be used”.*

Thus no requirement is specified for plate size correction, just that the plate size match the tire-contact area and pressure and that the same plate size be used for comparative analysis. Herein the 12 in. diameter plate was selected as the critical reference size, therefore  $F_{PlateSize} = 1.0$ .

### 2.1.2 Layered Analysis

Individual subgrade and base layer resilient modulus values were determined by obtaining resilient deflections measured at radii of 12 in. ( $2r$ ), 18 in. ( $3r$ ), and 24 in. ( $4r$ ) away from the plate center. The test setup is shown in Figure 3. The layered analysis measurement system was developed specifically for testing of unbound materials and provides average resilient deflections measured over one-third of the circumference of a circle at the selected radii. This method was designed to improve upon practices that use point measurements, which are often variable from point-to-point for unbound aggregate materials.

Eq. (3) as suggested by AASHTO (1993) can be used to determine subgrade layer resilient modulus value:

$$M_{r(sg)} = \frac{(1 - \nu^2) \cdot P}{\pi \cdot r' \cdot \delta_{r,r'}} \quad (3)$$

where,

$M_{r(sg)}$  is in-situ subgrade resilient modulus (psi),

$\delta_{r,r'}$  is the resilient deflection (in.) during the unloading portion of the cycle at  $r' = 2r$  or  $3r$  or  $4r$  away from plate center,

$\nu$  is the Poisson ratio (assumed as 0.40),

P is the cyclic load (lbs)



**Figure 3. APLT test setup with deformation measurements obtained at  $2r$ ,  $3r$ , and  $4r$  from the plate center axis.**

Per AASHTO (1993) and Ullidtz (1987), the lowest of the  $M_{r(sg)}$  values obtained from  $2r$ ,  $3r$ , and  $4r$  measurements using Eq. (3) was used to determine the subgrade  $M_r$ .

Ullidtz (1987) described Odemark's method of equivalent thickness (MET) concept, as illustrated in Figure 4, which shows a two-layered system on the left part with different moduli values for each layer.  $M_{r1}$  represents the resilient modulus of the top layer,  $M_{r2}$  represents the resilient modulus of the bottom layer, and  $h$  represents the thickness of the top layer. The Odemark's MET concept is that the top layer is transformed into a layer of equivalent thickness  $h_e$  with properties of the bottom layer (Ullidtz 1987). The  $h_e$  is calculated using Eq. (4), which can be simplified to Eq. (5), if Poisson's ratio ( $\nu$ ) is assumed as the same for the two layers:

$$h_e = h \times \sqrt[3]{\frac{M_{r1}(1-\nu_1^2)}{M_{r2}(1-\nu_2^2)}} \quad (4)$$

$$h_e = h \times \sqrt[3]{\frac{M_{r1}}{M_{r2}}} \quad (5)$$

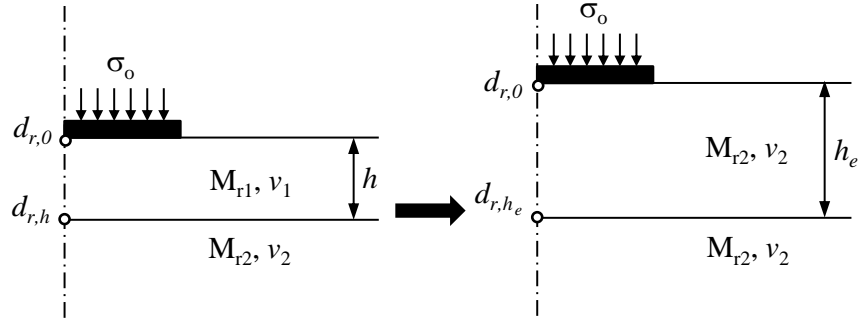


**Figure 4. Illustration of Odemark's MET concept.**

Using the Boussinesq's solution for linear-elastic materials and Odemark's MET method, Eq. (6) from AASHTO (1993) can be solved to determine the resilient modulus of the base layer ( $M_{r(base)}$ ):

$$\delta_c = (1-\nu^2) \sigma_o r f \left[ \frac{1}{M_{r(sg)} \sqrt{1 + \left( \frac{h}{r} \times \sqrt[3]{\frac{M_{r(base)}(1-\nu_1^2)}{M_{r(sg)}(1-\nu_2^2)}} \right)^2}} + \frac{\left( 1 - \frac{1}{\sqrt{1 + \left( \frac{h}{r} \right)^2}} \right)}{M_{r(base)}} \right] \quad (6)$$

where,

$\nu_1$  and  $\nu_2$  are Poisson ratio's for base and subgrade layer, respectively (assumed as 0.40 for both), and

$h$  is the thickness of the base layer (in.).

Past research has shown that stress measurements in two-layer systems of aggregate base over compressible subgrade are very similar to those

predicted by Boussinesq's analysis (e.g., McMahon and Yoder, 1960; Sowers and Vesic, 1961).

The two-layered analysis using the Odemark method is applicable for conditions with moduli values decreasing with depth (i.e., hard over soft), preferably by a factor of at least two between the consecutive layers (Ullidtz 1987). Ullidtz (1987) also noted that the  $h_e$  should be larger than the radius of the loading plate, i.e.,  $h_e/r > 1$ .

### 2.1.3 **Permanent Deformation Monitoring**

Permanent deformation results from cumulative plastic shear strain, compaction, and consolidation during loading. Permanent deformation ( $\delta_p$ ) was monitored during cyclic plate load testing at  $1r$ ,  $2r$ ,  $3r$ , and  $4r$ . From the number of load cycles ( $N$ ) versus  $\delta_p$  plot at  $1r$ , a deformation performance prediction model was developed to analyze and forecast the number of cycles to achieve a selected permanent deformation in the foundation layers. A power model was selected to represent the permanent deformation versus number of cycles as shown in Eq. 7:

$$\delta_p = CN^d \quad (7)$$

where, coefficient  $C$  is the plastic deformation after the first cycle of repeated loading, and  $d$  is the scaling exponent.

Monismith et al. (1975) described a similar power model relationship for relating permanent strain to cycle loadings for repeated triaxial laboratory testing. It is expected that  $C$  depends on the soil type, soil physical state, and stress conditions (See Li and Selig 1994) and  $d$  is expected to be relatively independent of these factors including resilient deflection.

The rate change of the permanent deformation is used herein to estimate the post-compaction permanent deformation and the corresponding number of loading cycles. Post-compaction permanent strain is a function of the shear stress magnitude and can reach an equilibrium state following the "shakedown" concept (see Dawson and Feller, 1999).

The in-situ traffic benefit ratio (TBR) (see Webster, 1992) or improvement to permanent deformation control, was calculated per Eq. (8):

$$TBR = \frac{N_{stabilized}}{N_{control}} \quad (8)$$

where,  $N_{stabilized}$  = number of load cycles to reach a certain permanent deformation in the stabilized section, and  $N_{control}$  = number of load cycles to reach a certain permanent deformation in the control section.

## 2.2 Dynamic Cone Penetration (DCP) Testing

DCP tests were performed in accordance with ASTM D6951-03 “Standard Test Method for Use of the Dynamic Cone Penetrometer in Shallow Pavement Applications”. The tests involved dropping a 17.6 lb hammer from a height of 22.6 in. and measuring the resulting penetration depth. A 30 in. penetrating rod was used. California bearing ratio (CBR) values were determined using Eqs. (9) and (10), whichever is appropriate, where the dynamic penetration index (*DPI*) is in units of mm/blow.

$$CBR(\%) = \frac{292}{DPI^{1.12}} \text{ for all materials except CL soils with CBR } < 10 \quad (9)$$

$$CBR(\%) = 1/(0.017019 \times DPI)^2 \text{ for CL soils with CBR } < 10 \quad (10)$$

## 2.3 In Situ Moisture and Density Testing

Moisture and dry density of the aggregate base layer at APLT locations were determined using sand cone testing in accordance with ASTM D1556/1556M-15 “Standard Test Method for Density and Unit Weight of Soil in Place by Sand-Cone Method”. A picture of an excavated hole at a test location ready for sand cone testing is shown in Figure 5.

Laboratory one-point standard Proctor test was conducted on the aggregate base material at its average in situ moisture content. Proctor compaction was conducted in accordance with ASTM 698-12e1 “Standard Test Methods for Laboratory Compaction Characteristics of Soil Using Standard Effort (12,400 ft-lb/ft<sup>3</sup> (600 kN-m/m<sup>3</sup>)).” Method C was followed.

Based on the dry density value determined from laboratory testing at the in situ moisture content, percent compaction was determined for field dry density measurements as the ratio of the field dry density and one-point laboratory dry density.



**Figure 5. Picture of an excavated hole ready for sand cone testing.**

## **2.4 Laboratory Testing**

### **2.4.1 Soil Index Properties**

Laboratory tests were performed on bulk samples of aggregate base and subgrade materials obtained from the test section, to determine the soil gradation parameters and soil classification.

The soil grain-size analysis test was conducted in accordance with ASTM C136M-14 “Standard Test Method for Sieve Analysis of Fine and Coarse Aggregates”. Atterberg limits tests were conducted in accordance with ASTM D4318-10e01 “Standard Test Methods for Liquid Limit, Plastic Limit, and Plasticity Index of Soils”. Tests were conducted using the multi-point method.

Using the grain-size analysis and Atterberg limits test results, the material was classified in accordance with ASTM D2487-11 “Standard Practice for Classification of Soils for Engineering Purposes (Unified Soil Classification System)” and ASTM D3282-09 “Standard Practice for Classification of Soils and Soil-Aggregate Mixtures for Highway Construction Purposes”.

### 2.4.2 Resilient Modulus

Laboratory  $M_r$  testing was performed on “undisturbed” shelly tube sample obtained from the subgrade layer immediately beneath the aggregate base layer and a reconstituted sample of aggregate base.

The 2.8 in. diameter sample was extruded from the tube and was trimmed to a height of about 5.6 in.  $M_r$  tests were conducted in accordance with AASHTO T-307 (2000) following the test sequence recommended therein for subgrade soils. The test involves one conditioning sequence with 500-1000 cycles followed by 15 loading sequences, with confining stresses ( $\sigma_c$ ) ranging from 2 to 6 psi and deviator stresses ( $\sigma_d$ ) ranging from 2 to 10 psi.

Two non-linear constitutive models were fit to the  $M_r$  test results for the subgrade material. One model used is the simple deviator stress model (also known as the  $k$ - $\sigma_d$  model) proposed by Moosazadeh and Witczak (1981), which is appropriate for cohesive soils:

$$M_r = k_1 \left( \frac{\sigma_d}{P_a} \right)^{k_2} \quad (11)$$

where,

$P_a$  = atmospheric pressure (psi),

$\sigma_d$  = deviator stress (psi), and

$k_1$  and  $k_2$  = regression coefficients.

Also, Witczak and Uzan (1988) proposed the  $k_1$ - $k_3$  or also known as the “universal” model which combines the effects of bulk and shear stresses into a single constitutive model:

$$M_r = k_1 P_a \left( \frac{\sigma_B}{P_a} \right)^{k_2} \left( \frac{\tau_{oct}}{P_a} + 1 \right)^{k_3} \quad (12)$$

where,

$\sigma_B$  = bulk stress (psi) =  $\sigma_1 + \sigma_2 + \sigma_3$ ,

$$\tau_{\text{oct}} = \text{octahedral shear stress (psi)} = \frac{\sqrt{(\sigma_1 - \sigma_2)^2 + (\sigma_2 - \sigma_3)^2 + (\sigma_3 - \sigma_1)^2}}{3}$$

$\sigma_1, \sigma_2, \sigma_3$  = principal stresses (psi), and

$k_1, k_2, k_3$  = regression coefficients.

In the “universal model”, the  $k_1$  coefficient is proportional to  $M_r$  and therefore is always  $> 0$ . The  $k_2$  coefficient explains the behavior of the material with changes in the bulk stresses. Increasing bulk stresses increases the  $M_r$  value and therefore the  $k_2$  coefficient should be  $\geq 0$ . The  $k_3$  coefficient explains the behavior of the material with changes in shear stresses. Increasing shear stress softens the material and decreases the  $M_r$  value. Therefore the  $k_3$  coefficient should be  $\leq 0$ .

The aggregate base material sample was compacted by preparing the material at the average moisture content to the average dry density determined from the field measurements. 4.0 in. diameter by 8 in. height sample was prepared and tested in accordance with AASHTO T-307 (2000) following the test sequence recommended therein for base/subbase materials. The test involves one conditioning sequence with 500-1000 cycles followed by 15 loading sequences, with confining stresses ( $\sigma_c$ ) ranging from 3 to 20 psi and deviator stresses ( $\sigma_d$ ) ranging from 3 to 40 psi.

Two non-linear constitutive models were fit to the  $M_r$  test results for the aggregate base material. One is the universal model described above in Eq. (12) and the other is the simple bulk stress model (also known as the K- $\theta$ ) model proposed by Seed et al. (1967) for granular materials:

$$M_r = k_1 \left( \frac{\theta}{P_a} \right)^{k_2} \quad (13)$$

where,  $\theta$  = bulk stress =  $\sigma_1 + \sigma_2 + \sigma_3$ .

## 3 Experimental Study

### 3.1 Field Experimental Study

For this project, the field testing program involved conducting cyclic APLTs with seven loading sequences. Table 1 provides details of the APLT configuration, number of load cycles, and cyclic stresses used in this study.

**Table 1. Summary of plate tests and configurations.**

Load Sequence	Number of Load Cycles	Target Stress Range (psi)		Plate Configuration/Notes
		Min	Max	
1	100 (conditioning)	2	5	12 in. diameter, flat plate including deflection readings @ 2r, 3r, and 4r.
2	100	2	10	
3	100	2	20	
4	100	2	40	
5	100	2	60	
6	100	2	80	
7	100	2	100	

The sections in this study contained geogrids between the aggregate base layer at the surface and the underlying untreated subgrade. The properties those geogrids are shown in Figure 6 and their properties are identified in Table 2.

**Table 2. Summary of geogrid mechanical properties.**

Geogrid	Type	Index Properties
TX130s	Multi-axial geogrid with hexagonal structure and triangular apertures	Rib pitch longitudinal and diagonal 1.3 inch
BX1200	Bi-axial geogrid with square apertures	Aperture dimension 1 in and flexural stiffness 750,000 mg-cm

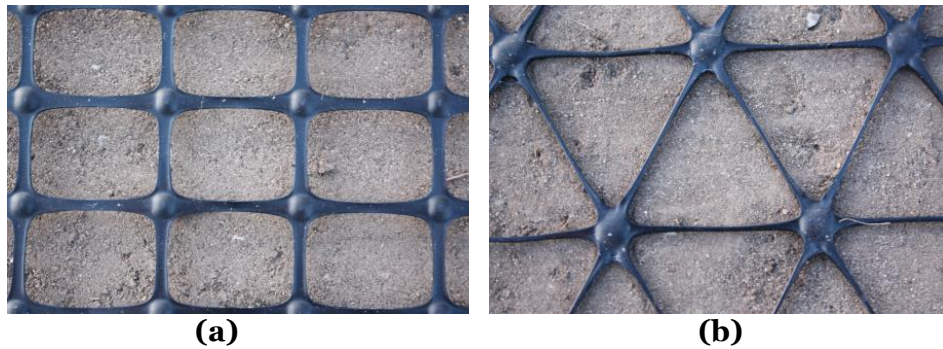


**Figure 6. Pictures of geogrids used in this study during construction of test sections in 2012: (a) BX1200 and (b) TX130s (field of view for each image about 4 inches).**

The results presented herein represent a selected number of measurements per sample group that was feasible for the site conditions and/or time available for testing. Statistical determination of the minimum number of measurements requires knowledge of the coefficient of variation within a sample group and the difference between mean values of the selected sample groups. Determination of statistical input parameters needed for calculating statistical sample sizes was beyond the scope of this study.

## **3.2 Project Details**

### **3.2.1 Test Section Construction and 2012 Testing**

The test sections were initially constructed in 2012 over a relatively flat area of about 65 ft x 100 ft. Construction details of the test sections are provided in White (2013). A truck trafficking study was conducted in 2012, which involved making multiple passes using a loaded truck over the test sections and measuring the rut depths in the wheel tracks. Results from the truck trafficking study were used to determine the number of passes (N) required to achieve 2 inches of maximum deflection in the stabilized and the control sections. The N values were used to calculate the TBR values for comparison with the current APLT testing.

TBR results are summarized in Table 3, which indicates that both TX130s and BX1200 geogrid sections showed  $TBR > 4$ .

**Table 3. Summary of TBR in the geogrid stabilized sections from 2012 trafficking tests.**

<b>Geogrid</b>	<b>N to reach 2 in. maximum defl.</b>	<b>TBR</b>
Control	11.2	—
TX130s	47.6	4.3
BX1200	46.1	4.1

### **3.2.2 2015 Testing**

Just prior to testing, the surface of all test sections was fine graded in the top 0.5 inch and recompactd using approximately 6 passes of a vibratory plate compactor to obtain a level and compacted testing surface for APLT (Figure 7). Pictures of aggregate base material at the surface and APLT setup are shown in Figure 8 and Figure 9, respectively. The surface was smooth, level, and tight with no loose aggregate.



**Figure 7. Vibratory compaction of aggregate base layer prior to APLT for uniform and level testing surface.**



**Figure 8. Aggregate base layer surface at the time of testing.**



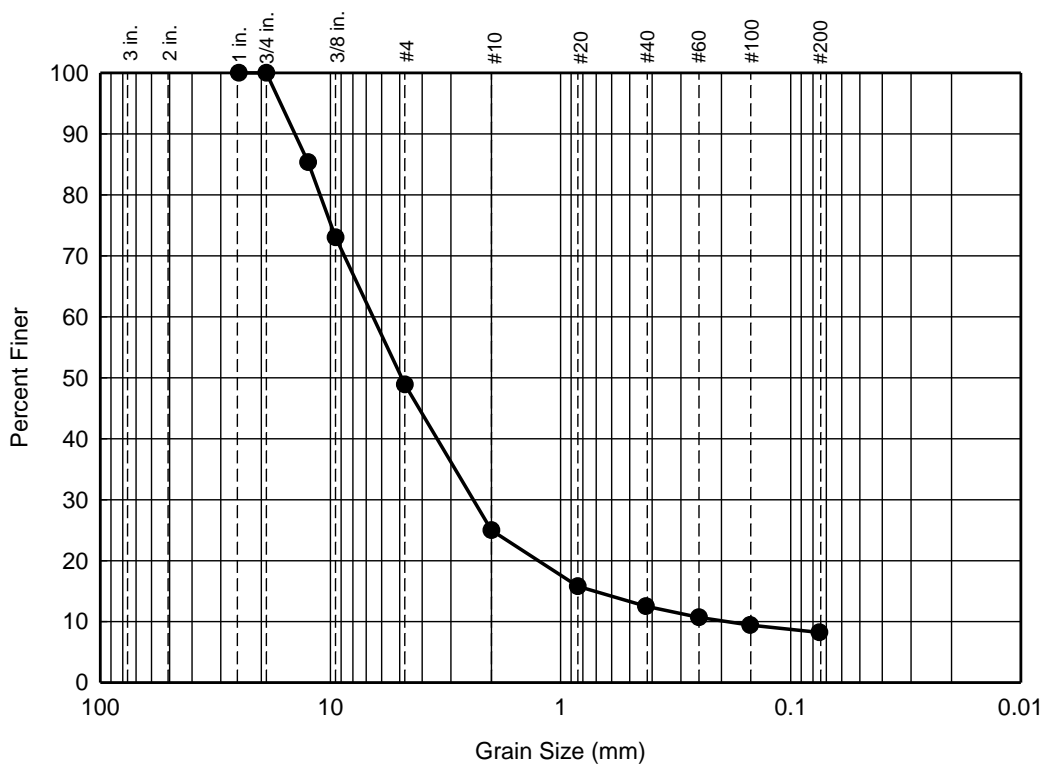
**Figure 9. APLT setup showing 12 in. diameter plate and the 2r, 3r, and 4r deflection basis measurement rings.**

### **3.3 Material Properties and Laboratory Test Results**

The aggregate base material consisted of crushed limestone material. Grain-size analysis test and soil classification results for the base material are provided in Figure 10. Pictures of the loose material used in particle-size analysis and gravel size material (coarser than No. 4 sieve) are shown in Figure 11. The material consisted of 100% passing the  $\frac{3}{4}$  in. sieve with about

8% fines passing the No. 200 sieve, and classified as GP-GM according to USCS and A-1-a according to AASHTO classifications.

The subgrade material directly beneath the subgrade consisted of dark brown glacial till material. Grain-size analysis test and soil classification results for the subgrade material are provided in Figure 12. The material consisted of about 55% fines (silt + clay) passing the No. 200 sieve and about 45% sand. It classified as CL (sandy lean clay) according to USCS and A-6(4) according to AASHTO classifications.



% Gravel		% Sand			% Fines
Coarse	Fine	Coarse	Medium	Fine	Silt + Clay
0.0	51.1	23.9	12.5	4.3	8.2

Gradation Parameters						
D <sub>10</sub> = 0.197	D <sub>30</sub> = 2.576	D <sub>50</sub> = 4.967	D <sub>60</sub> = 6.936	D <sub>85</sub> = 12.416	c <sub>u</sub> = 35.225	c <sub>c</sub> = 4.858

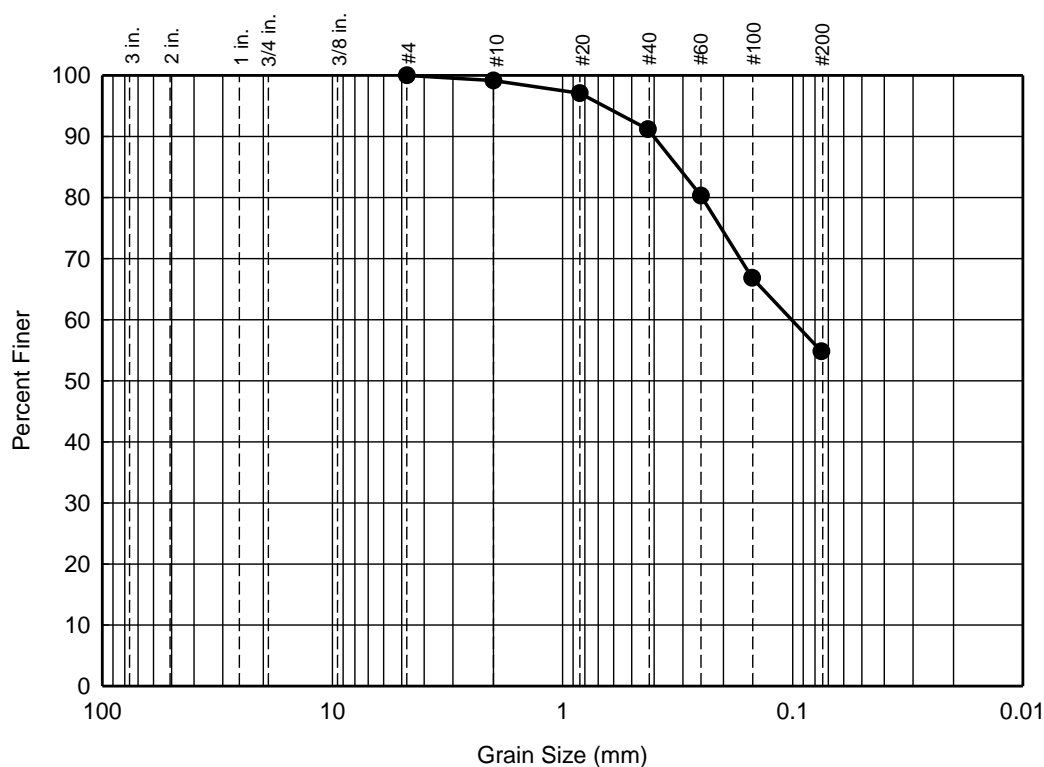
  

Atterberg Limits			Classification	
PL = NP	LL = NP	PI = NP	USCS = GP-GM Poorly graded gravel with sand and silt	AASHTO = A-1-a

**Figure 10. Grain-size analysis and classification of the crushed limestone aggregate base material.**



**Figure 11. (top) Full gradation sample and (bottom) gravel retained on No. 4 sieve after washing and oven-drying for the crushed aggregate base material.**



% Gravel		% Sand			% Fines
Coarse	Fine	Coarse	Medium	Fine	Silt + Clay
0.0	0.0	0.8	8.0	36.4	54.8

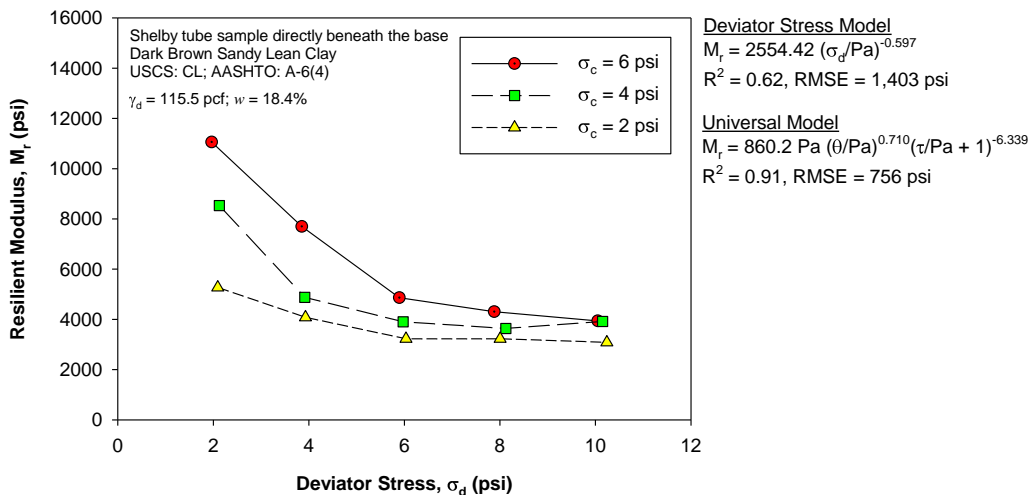
  

Atterberg Limits			Classification	
PL = 18	LL = 30	PI = 12	USCS = CL (Sandy Lean Clay)	
			AASHTO = A-6(4)	

**Figure 12. Grain-size analysis and classification of the subgrade material directly beneath the aggregate base.**

Laboratory  $M_r$  tests were conducted on a Shelby tube sample obtained from the subgrade directly beneath the aggregate base layer.  $M_r$  test results are presented in Figure 13, along with the prediction expressions for the deviator stress ( $k-\sigma_d$ ) and “universal” ( $k_1-k_3$ ) models. The dry density of the material ( $\gamma_d$ ) was about 115.5 pcf at a moisture content ( $w$ ) of about 18.4%.

The test results indicate that that  $M_r$  decreases as  $\sigma_d$  increases and  $\sigma_c$  decreases. For this dataset, the “universal” model produced higher coefficient of determination ( $R^2$ ) and lower root mean squared error (RMSE) compared to the  $k-\sigma_d$  model.



**Figure 13. Results of laboratory  $M_r$  testing on subgrade sample and prediction equations based using  $k$ - $\sigma_d$  and  $k_1$ - $k_3$  constitutive models**

$M_r$  test results on the compacted aggregate sample are presented in Figure 13, along with the prediction expressions for the bulk stress ( $k$ - $\theta$ ) and “universal” ( $k_1$ - $k_3$ ) models. The dry density of the material ( $\gamma_d$ ) was about 116.6 pcf at a moisture content ( $w$ ) of about 2.3%, which were close to the average field dry density and moisture content.

The test results indicate that that  $M_r$  increases as bulk stress increases. For this dataset, the “universal” model produced higher coefficient of determination ( $R^2$ ) and lower root mean squared error (RMSE) compared to the  $k$ - $\theta$  model. This is expected as the  $k$ - $\theta$  model does not account for the shear stresses developed during loading as the “universal” model.

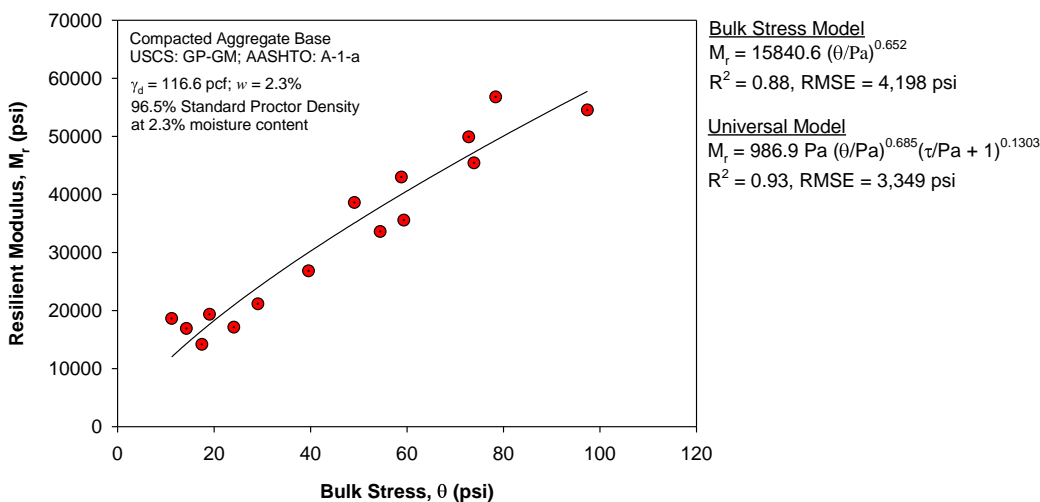


**Figure 14. Results of laboratory  $M_r$  testing on aggregate base and prediction equations based using  $k$ - $\theta$  and  $k_1$ - $k_3$  constitutive models.**

## 4 Results

### 4.1 Dynamic Cone Penetration (DCP) Test Results

Figure 15 shows the CBR and cumulative blows profiles at all test locations. The base layer was about 6 in. thick. The average CBR in the base layer varied from about 3.5 (Control 2) to 12 (BX1200). In the top 12 in. of the subgrade layer, the average CBR varied from about 0.7 (Control 1) to 2.3 (BX1200), representing soft subgrade conditions. The CBR in the subgrade generally decreased with increasing depth to  $< 1$  at all test locations.

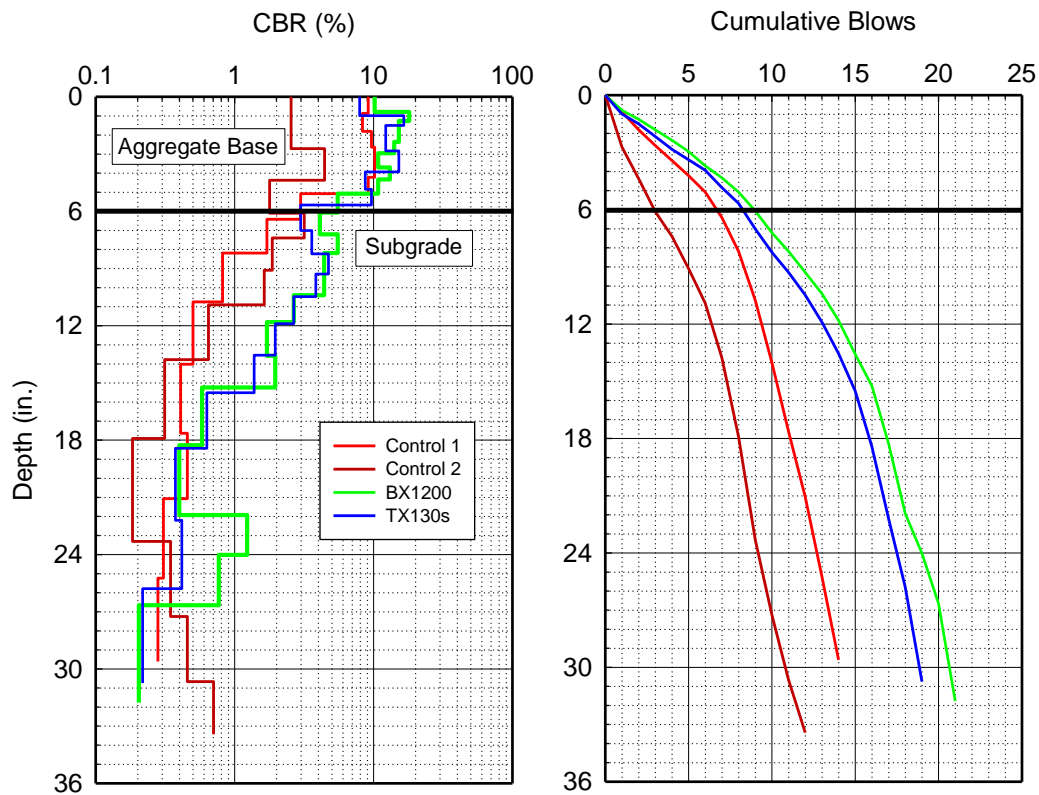


Figure 15. DCP profiles for all test locations.

## 4.2 Comparison of APLT Permanent Deformation Basins and Power Models

Figure 16 to Figure 19 present the permanent deformation,  $\delta_p$ , versus number of cycles for all test points, at  $1r$ ,  $2r$ ,  $3r$ , and  $4r$ , respectively.

Results indicated that the control sections showed the highest  $\delta_p$  with 1.1 to 1.5 in. at the end of 700 cycles. The TX130s section showed the lowest  $\delta_p$  (< 0.5 in.) while BX1200 section showed  $\delta_p = 0.75$  in., at the end of 700 cycles.

In the Control 2 section,  $\delta_p$  at  $2r$  and  $3r$  produced negative deformation values which represents a vertical heaving condition. Minor amounts of heave (<0.01 in.) were produced at the  $4r$  position in all sections except the TX130s section.

Permanent deformation deflection basins at the end of each loading sequence comparing all test locations are shown in Figure 20. The results show that for all sections there was minimal permanent deformation outside of the perimeter of the loading plate. This behavior is indicative of soft subgrade conditions where the plate deformations are governed by the permanent deformations. Figure 24 shows the ratio of  $\delta_p$  at  $2r$ ,  $3r$ , and  $4r$ , to  $\delta_p$  at  $1r$ , which represents the relative movements (on a percent basis). If the ratio is negative, it represents a plastic deformation/heave mode in the basin while the opposite represents a near-linear elastic/compression mode in the basin. At 500 cycles the results show that both TX130s and BX1200 geogrid sections were in near-linear elastic/compression mode while the Control sections were in plastic deformation/heave mode in the basin. The Control 2 section produced the most heave in the deflection basin region and the TX130s produced the most compression in the deflection basin region. This observation provides new understanding of the geogrid-subgrade-subbase interaction.

A summary of power model trafficking performance parameters ( $C$  and  $d$ ) per Eq. 7 for each cyclic stress level and test section is provided in Table 4. Using the  $C$  and  $d$  values and Eq. 7, the number of cycles to achieve 1.0 inch  $\delta_p$  were calculated and are summarized in Table 4. TBR are also provided in Table 4, which were calculated using the average  $N$  of the two control sections.

The TX130s section showed higher TBR values (4.1 to 5.4) than the BX1200 section (1.6 to 1.9) at  $\square_{\text{cyclic}} \geq 37$  psi. The TBR values determined from

APLT testing in the TX130s section are comparable to the TBR values measured from the 2012 truck trafficking testing. The TBR values from APLT testing in the BX1200 section, however, were lower than measured from the truck trafficking testing.

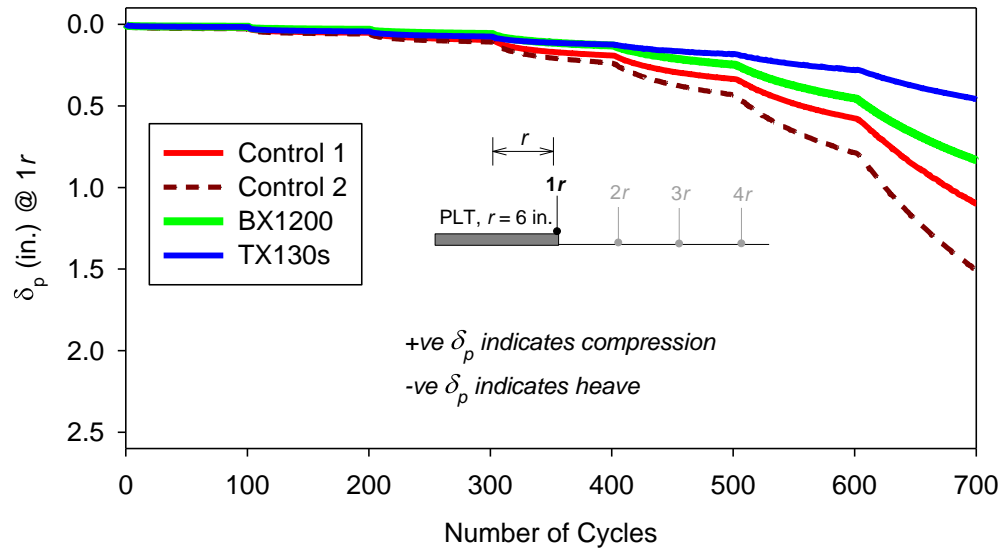


**Figure 16. Permanent deformation at  $1r$  versus load cycle number at all test points.**

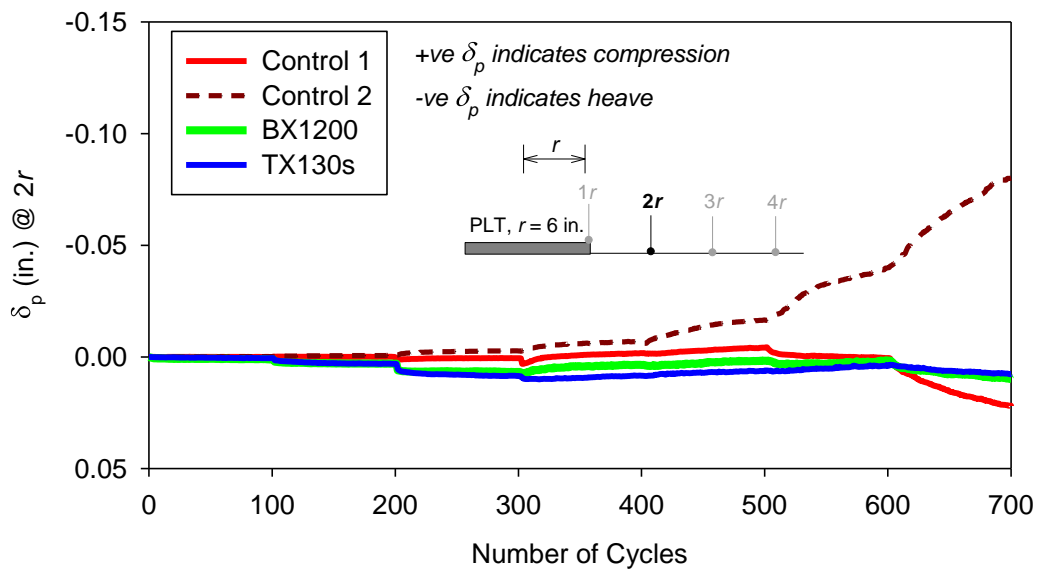


**Figure 17. Permanent deformation at  $2r$  versus load cycle number at all test points.**

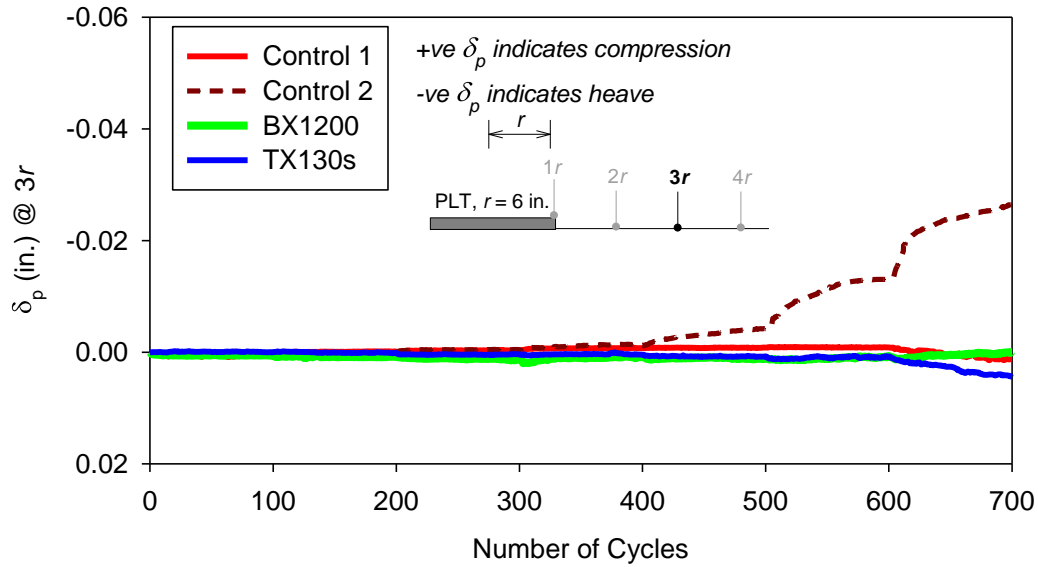


**Figure 18. Permanent deformation at  $3r$  versus load cycle number at all test points.**

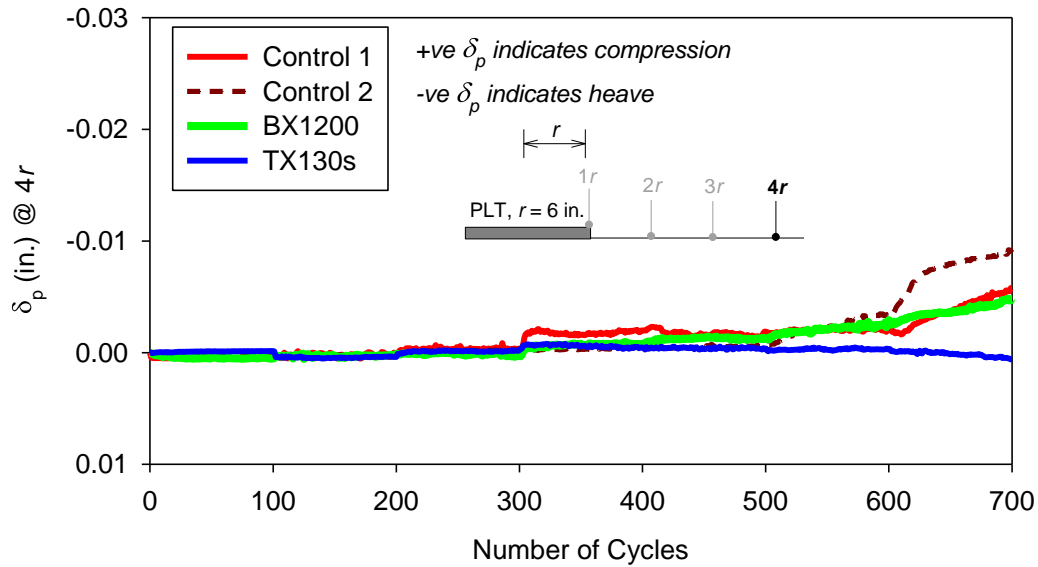


**Figure 19. Permanent deformation at  $4r$  versus load cycle number at all test points.**

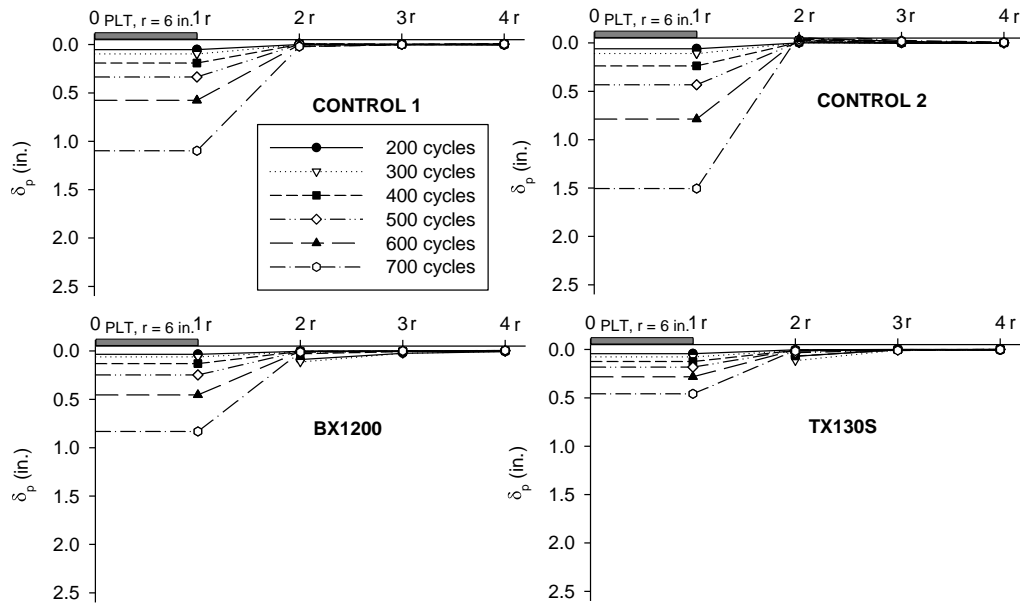


**Figure 20. Permanent deformation basins at all test points at the end of each load sequence.**

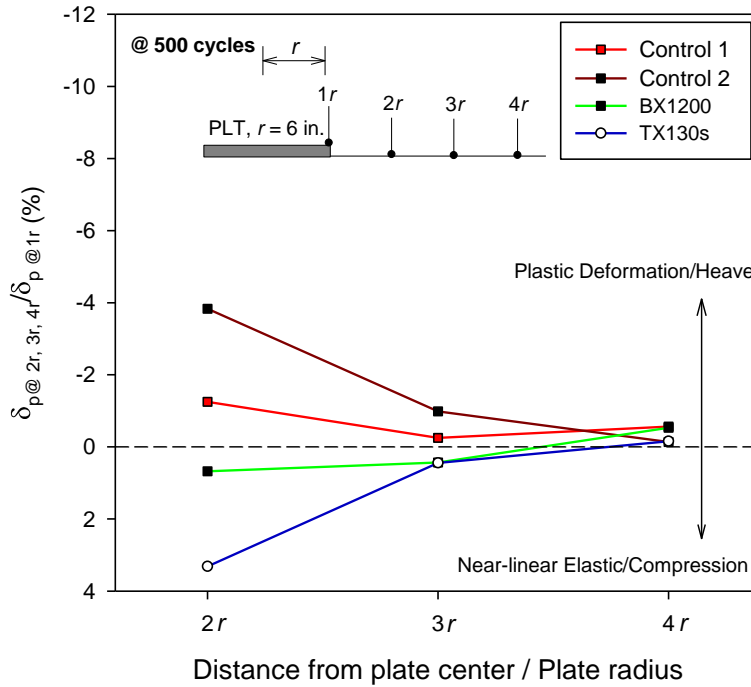


**Figure 21. Ratio of vertical permanent deformation with distance from plate edge showing near-linear elastic compression and plastic deformation modes at end of 500 cycle test sequence.**

**Table 4. Summary of permanent deformation prediction parameters.**

Section	$\sigma_{\text{cyclic}}$ (psi)	$C$	$d$	$R^2$	N at $\delta_p =$ 1 in.	TBR
Control 1	8.2	0.0097	0.2504	0.9954	> 10,000,000	N/A
	17.3	0.0070	0.4005	0.9989	240,176	
	37.0	0.0124	0.4466	0.9943	18,582	
	57.2	0.0088	0.6127	0.9953	2,264	
	77.9	0.0085	0.7334	0.9963	666	
	97.0	0.0100	0.8658	0.9988	204	
Control 2	8.2	0.0113	0.2316	0.9911	> 10,000,000	N/A
	17.3	0.0102	0.3464	0.9900	560,847	
	37.0	0.0173	0.4407	0.9931	9,956	
	57.2	0.0105	0.6400	0.9951	1,236	
	77.9	0.0124	0.7348	0.9960	393	
	97.0	0.0146	0.8530	0.9980	142	
BX1200	8.2	0.0077	0.1974	0.9955	> 10,000,000	279.2
	17.3	0.0047	0.3717	0.9885	1,831,691	4.6
	37.0	0.0081	0.4728	0.9956	26,526	1.9
	57.2	0.0064	0.6360	0.9968	2,815	1.6
	77.9	0.0075	0.7248	0.9977	855	1.6
	97.0	0.0084	0.8289	0.9983	319	1.8
TX130s	8.2	0.0092	0.2415	0.9515	> 10,000,000	1.5
	17.3	0.0064	0.3466	0.9934	2,135,720	5.3
	37.0	0.0063	0.4502	0.9907	77,300	5.4
	57.2	0.0029	0.6588	0.9943	7,110	4.1
	77.9	0.0037	0.7181	0.9962	2,435	4.6
	97.0	0.0042	0.8249	0.9985	761	4.4

### 4.3 In-Situ Resilient Modulus

Figure 22 presents the resilient deflection ( $\delta_r$ ) basins at the end of the each loading sequence (after 200, 300, 400, 500, 600, and 700 cycles). Using the  $\delta_r$  at  $1r$ , composite  $M_r$  values were calculated. Using the  $\delta_r$  at  $2r$ ,  $3r$ , and  $4r$ , layered analysis was conducted to determine subgrade ( $M_{r(sg)}$ ) and base layer ( $M_{r(\text{Base})}$ ). A summary of  $M_r$  values for each loading sequence (determined as the average of the last five cycles),  $\delta_p$  at the end of each loading sequence, and the  $h_e/r$  values are presented in Table 5.

As summarized in Table 5, some loading sequences and test locations resulted in  $h_e/r$  ratio  $< 1$  and were therefore not considered to meet the Odemark's analysis requirements (see section 2.1.2). Also, those points produced plastic deformation/heave in the deflection basins as shown in Figure 21, which does not qualify the near-linear elastic behavior that is assumed in the Odemark's layered analysis.

Results indicated that the composite  $M_r$ ,  $M_{r(sg)}$ , and  $M_{r(Base)}$  values decreased with increased cyclic stresses. This behavior was also observed in laboratory  $M_r$  testing on the subgrade material. The opposite was observed in laboratory testing on the base material. The composite  $M_r$  values at  $\sigma_{cyclic} = 98$  psi ranged between 6.1 ksi and 8.7 ksi in all sections. The composite  $M_r$  values were similar to the  $M_{r(sg)}$  values in all sections, especially at  $\sigma_{cyclic} > 30$  psi, which suggests that the composite behavior is dominated by the subgrade layer stiffness.

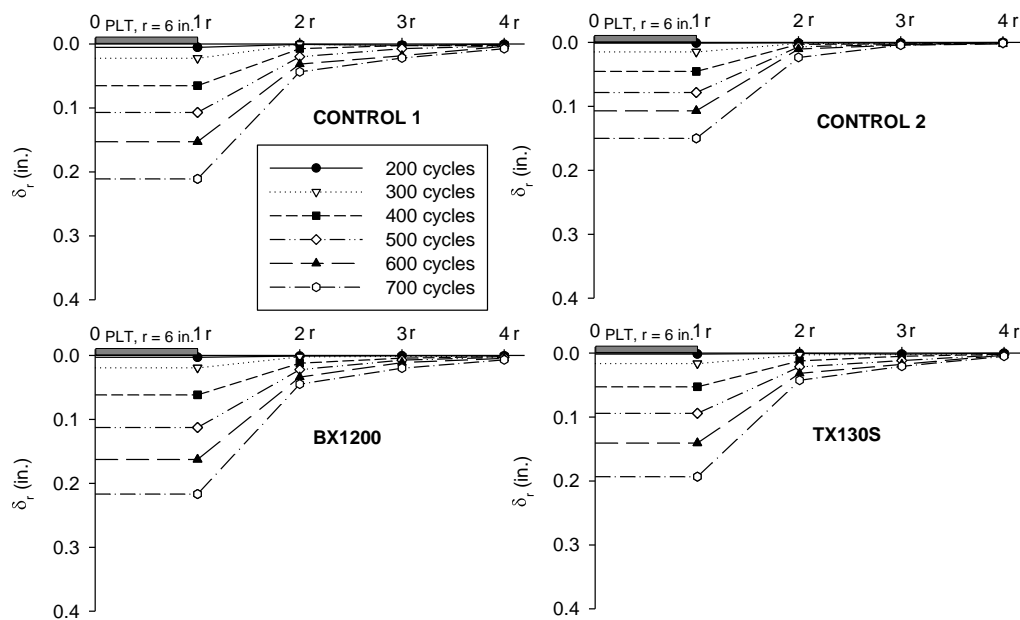


**Figure 22. Resilient deformation basins at all test points at the end of each load sequence.**

**Table 5. Comparison of test results for in-situ  $M_r$  and permanent deformation testing.**

Test Section	Cycles	$\sigma_{\text{cyclic}}$ (psi)	$M_r$ (psi)	$M_r$ (sg) (psi)	$M_r$ (Base) (psi)	$h_e/r$	$\delta_p$ (in.)
Control 1	195-200	8.2	21,503	8,938	117,326	2.36	0.052
	295-300	18.0	9,563	—*	—*	< 1.0	0.096
	395-400	37.8	7,848	—*	—*	< 1.0	0.192
	495-500	57.9	7,259	—*	—*	< 1.0	0.336
	595-600	77.6	6,815	6,253	7,753	1.07	0.579
	695-700	97.5	6,205	5,666	7,113	1.08	1.097
Control 2	195-200	8.2	89,596	35,917	524,037	2.44	0.059
	295-300	17.3	16,265	—*	—*	< 1.0	0.108
	395-400	38.1	11,221	—*	—*	< 1.0	0.238
	495-500	56.6	9,842	—*	—*	< 1.0	0.433
	595-600	77.1	9,333	—*	—*	< 1.0	0.788
	695-700	98.7	8,729	—*	—*	< 1.0	1.500
TX130s	195-200	8.1	75,564	37,915	272,446	1.93	0.044
	295-300	17.6	14,677	—*	—*	< 1.0	0.075
	395-400	36.5	9,374	7,730	12,710	1.18	0.124
	495-500	57.7	8,128	6,761	10,857	1.17	0.182
	595-600	76.3	7,309	6,117	9,662	1.16	0.282
	695-700	99.0	6,893	5,879	8,828	1.15	0.457
BX1200	195-200	8.3	39,337	26,379	78,281	1.44	0.034
	295-300	17.1	11,980	—*	—*	< 1.0	0.060
	395-400	36.7	8,134	7,926	8,446	1.02	0.130
	495-500	57.7	6,897	6,590	7,375	1.04	0.248
	595-600	77.9	6,422	5,830	7,430	1.08	0.457
	695-700	98.5	6,103	5,555	7,031	1.08	0.831

\*  $h_e/r < 1.0$  therefore not compliant with Odemark's MET analysis;  $h_e$  per Eq. 5.

	Control 1	Control 2	BX1200	TX130s
As-built gravel layer thickness (in.)	6.0	6.0	6.0	6.0
Average Base CBR (%)*	8.9	3.5	12	11
Average Subgrade CBR (%) (12 in.)	0.7	1.0	2.3	2.2
In-Situ $M_r$ (psi) at $\sigma_{cyclic} = 98$ psi	6,205	8,729	6,103	6,893
In-Situ Dry Density, $\gamma_d$ (pcf)	109.6	—	120.1	119.2
In-Situ Moisture Content, $w$ (%)	2.2	—	2.0	2.4
Permanent Def. after 700 cycles, $\delta_p$ (in.)	1.106	1.505	0.831	0.458

\* DCP tests unconfined at surface.

**Figure 23. Summary of aggregate layer thicknesses and in-situ measurement values.**

## 5 Conclusions and Recommendations

A summary of the key observations from the tests conducted in this study are as follows:

1. The test sections selected for in-situ performance assessment and comparison of TX130s and BX1200 geogrid test sections, provided an excellent opportunity to evaluate the stabilized aggregate base layers over relatively soft subgrade ( $\text{CBR} < 3$  and decreased with depth). The aggregate base course classified as poorly-graded gravel with sand and silt (GP-GM) with about 8% fines content and the subgrade layer classified as sandy lean clay (CL).
2. The control sections showed the highest  $\delta_p$  with 1.1 to 1.5 in. at the end of 700 cycles. The TX130s section showed the lowest  $\delta_p$  ( $< 0.5$  in.) while the BX1200 section showed  $\delta_p = 0.75$  in., at the end of 700 cycles.
3. The TX130s section showed higher TBR values (4.1 to 5.4) than the BX1200 section (1.6 to 1.9) at  $\sigma_{\text{cyclic}} \geq 37$  psi. The TBR values determined from APLT testing in the TX130s section are comparable to the TBR values measured from the 2012 truck trafficking testing. The TBR values from APLT testing in the BX1200 section, however, were lower than measured from the truck trafficking testing.
4. In the Control 2 section,  $\delta_p$  at  $2r$  and  $3r$  resulted in vertical heaving. Results from the remaining sections showed that there was little  $\delta_p$  outside the perimeter of the loading plate. This is indicative of soft subgrade conditions where the plate deformations are governed significantly by permanent deformations in the subgrade layer.
5. The permanent deformation basin values analyzed in terms of relative movements indicated that both TX130s and BX1200 geogrid sections were in near-linear elastic/compression mode while the control sections were in plastic deformation/heave mode. The Control 2 section produced the most heave in the deflection basin region and the TX130s produced the most compression in the deflection basin region. This observation provides new understanding of the geogrid-subgrade-subbase interaction.

6. The composite  $M_r$  and  $M_{r(\text{sg})}$  and  $M_{r(\text{Base})}$  values calculated from layered analysis, all decreased with increased cyclic stresses. This behavior was observed in laboratory  $M_r$  testing on the subgrade material. The opposite was observed for the aggregate laboratory resilient modulus test. The composite  $M_r$  values at  $\sigma_{\text{cyclic}} = 98$  psi ranged between 6.1 ksi and 8.7 ksi in all sections. The composite  $M_r$  values were similar to the  $M_{r(\text{sg})}$  values in all sections, especially at  $\sigma_{\text{cyclic}} > 30$  psi, which suggests that the composite behavior is dominated by the subgrade layer stiffness.
7. Additional testing is recommended for a moderate subgrade stiffness (CBR 3-7).

---

## References

- AASHTO T307-99 (2000). "Standard Method of Test for Determining the Resilient Modulus of Soils and Aggregate Materials", Standard Specifications for Transportation Materials and Methods of Sampling and Testing, Twentieth Edition, American Association of State Highway and Transportation Officials, Washington, DC.
- AASHTO T222-81 (2012). "Standard Method of Test for Nonrepetitive Static Plate Load Test of Soils and Flexible Pavement Components for Use in Evaluation and Design of Airport and Highway Pavements", Standard Specifications for Transportation Materials and Methods of Sampling and Testing, Thirty Second Edition, American Association of State Highway and Transportation Officials, Washington, DC.
- AASHTO (1993). *AASHTO Guide for Design of Pavement Structures*, Published by the American Association of State Highway and Transportation Officials, Washington, D.C.
- Brown, S., and Hyde, A. (1975). "Significance of cyclic confining stress in repeated-load triaxial testing of granular material." *Transportation Research Record*, (537).
- Collins, I.F., Wang, A. P. and Saunders, L.R. (1993). Shakedown theory and the desing of unbound pavements. *Road and Transport Research*, Vol. 2, No. 4, Dec. pp. 28-39.
- Houston, S. L., Perez-Garcia, N., and Houston, W., N. (2008). "Shear strength and shear-induced volume change behavior of unsaturated soils from triaxial test program." *Journal of Geotechnical and Geoenvironmental Engineering*, Vol. 134, No. 11, p. 1619-1632.
- Kim, K., Lee, S., Park, Y., Kim, S. (2012). "Evaluation of Size Effects of Shallow Foundation Settlement Using Large Scale Plate Load Test," *Journal of Korean Geotechnical Society*, 28(7), 67-75.
- LeKarp, F., Isacsson, U., and Dawson, A. (2000). "State of the art. I: Resilient response of unbound aggregates." *Journal of Transportation Engineering*, American Society of Civil Engineers.

- 
- Li, D., and Selig, E. T., (1994). Resilient modulus for fine-grained subgrade soils." *J. Geotech. Engrg.*, ASCE, 120(6), 939-957.
- McMahon, T. F., and E.J. Yoder, (1960). "Design of a pressure sensitive cell and model studies of pressures on a flexible pavement subgrade." Proceedings, *Highway Research Board*, Vol. 39, pp. 650-682.
- Monismith, C.L., Ogawa, N., and Freeme, C. R. (1975). "Permanent deformation characteristics of subgrade soils due to repeated loading." *Transportation Research Record*, 537, 1-17.
- NCHRP. (2004). "Laboratory Determination of Resilient Modulus for Flexible Pavement Design," Research Results Digest Number 285, National Cooperative Highway Research Program, Transportation Research Board, Washington, D.C.
- Seed, H.B., Mitry, F.G., Monismith, C.L., and Chan, C.K. (1967). "Prediction of pavement deflection from laboratory repeated load tests", NCHRP Report 35, Transportation Research Board, Washington, D.C., USA.
- Sowers, G. F., and A. B. Vesic. (1961). "Stress distribution beneath pavements of different rigidities." Proceedings, *International Conference on Soils Mechanics and Foundation Engineering*, 5<sup>th</sup>, vol. 2, pp. 327-332
- Ullidtz, P. (1987). *Pavement Analysis*, Elsevier, New York, NY.
- Webster, S. L. (1992). "Geogrid reinforced base courses for flexible pavements for light aircraft: Test section construction, behavior under traffic, laboratory tests, and design criteria." *Final Rep.*, DOT/FAA/RD-92/25, U.S. Dept. of Trans and Fed. Aviation Admin., Washington, D.C., 91.
- Werkmeister, S., Dawson, A., and Wellner, F. (2013). "Permanent deformation behavior of granular materials and the shakedown concept." Transportation Research Record, No. 1757, *Journal of the Transportation Research Board*, p. 75-81
- White, D.J. (2013). "Technology Development Report: Automated Plate Load Test System Assessment of Geosynthetic Reinforcement Aggregate Base," *Interim Report*, GeoMatters, Inc., Boone, Iowa, USA.

White, D. J. (2015). "Field Evaluation of Plate Size Corrections for Cyclic Plate Load Testing: Geogrid Stabilized Aggregate Base over Soft Subgrade," *Interim Report*, Ingios Geotechnics, Inc. Boone, Iowa, USA.